Differences in Conformation and Conformational Dynamics Between Cisplatin and Oxaliplatin DNA Adducts

Stephen G. Chaney, Srinivas Ramachandran, Shantanu Sharma, Nikolay V. Dokholyan, Brenda Temple, Debadeep Bhattacharyya, Yibing Wu, and Sharon Campbell

Abstract Some DNA damage-recognition proteins, transcription factors, mismatch repair proteins and DNA polymerases discriminate between cisplatin (CP)- and oxaliplatin (OX)-GG DNA adducts, and this is thought to help explain differences in efficacy, toxicity and mutagenicity of CP and OX. In addition, differential recognition of CP- and OX-GG adducts by some proteins has been shown to be highly dependent on the sequence context of the Pt-GG adduct. We have postulated that CP- and OX-GG adducts cause differences in the conformation and/or conformational dynamics of the DNA that provide the basis for differential protein recognition of the adducts. We have determined the NMR solution structure of CP-GG adducts, OX-GG adducts and undamaged DNA in the AGGC sequence context, and of OX-GG adducts and undamaged DNA in the TGGT sequence context. We have also employed molecular dynamics (MD) simulations to investigate the conformational dynamics of CP-GG adducts, OX-GG adducts and undamaged DNA in the AGGC and TGGA sequence contexts. These studies showed clear differences in the conformation dynamics between CP- and OX-GG adducts which correlated with the average conformational differences observed in the NMR solution structures and with conformations previously reported for the CP-GG DNA·HMG1a complex. When the conformational dynamics in both sequence contexts were compared it became evident that: (a) the patterns of hydrogen bond formation between Pt-amine-hydrogens and surrounding bases of the DNA were different for CP- and OX-GG adducts; (b) patterns of hydrogen bond formation were also influenced by the DNA sequence context of the Pt-GG adducts, and (c) differences in patterns of hydrogen bond formation were highly correlated with differences in the conformational dynamics of the adduct. Thus, we postulate that patterns of hydrogen bond formation between Pt-amine hydrogens and surrounding DNA bases are different for CP- and OX-GG adducts, and that those differences in hydrogen bond patterns result in DNA conformational differences that allow selective recognition of CP- and

S.G. Chaney (✉), S. Ramachandran, S. Sharma, N.V. Dokholyan, B.Temple, D. Bhattacharyya, Y. Wu, and S. Campbell
Department of Biochemistry and Biophysics, School of Medicine, University of North Carolina, Chapel Hill, NC, USA
e-mail : stephen_chaney@med.unc.edu

A. Bonetti et al. (eds.), *Platinum and Other Heavy Metal Compounds in Cancer Chemotherapy*, DOI: 10.1007/978-1-60327-459-3_20,

OX-GG adducts by a number of proteins that determine the relative cytotoxicity and mutagenicity of those adducts.

Keywords Cisplatin; Oxaliplatin; DNA adducts; Conformational dynamics; DNA damage and repair

Introduction

Cisplatin [CP, *cis*-diamminedichloroplatinum(II)] and carboplatin [CBDCA, *cis*-diammine-1,1-cyclobutanedicarboxylatoplatinum(II)] are widely used in treating several types of cancers such as ovarian, testicular, head and neck tumors. However, many tumors show resistance or develop acquired resistance towards CP or CBDCA. Tumors that are resistant to these drugs are usually cross-resistant to the other drug. CP also exhibits mutagenic properties in vivo (1) which have been associated with secondary malignancies (2). Oxaliplatin [OX, *trans*-(*R,R*)-1,2-diaminocyclohexaneoxalatoplatinum(II)] is a third-generation platinum anticancer agent and has been approved for treatment of colorectal cancer and cisplatin-resistant tumors. While OX does exhibit some mutagenicity (3), it is less mutagenic than CP (4). Although the reasons for differences in tumor range and mutagenicity of OX compared to those of CP and CBDCA are not known, these differences are thought to be determined by the discriminating ability of proteins that are involved in damage recognition, damage repair, and/or damage tolerance. For example, hMSH2 and MutS bind with greater affinity to CP-GG adducts than to OX-GG adducts (5, 6), and defects in mismatch repair result in resistance to CP and CBDCA, but not to OX (5, 7–10). In addition, several transcription factors and damage recognition proteins have been shown to discriminate between CP- and OX-GG adducts (11, 12). The binding specificity has been determined for only a few of these proteins, but where it has been studied, they bind to CP-GG adducts with higher affinity than to OX-GG adducts (11–13). Moreover, translesion DNA polymerases such as pol β and pol η have been shown to bypass OX-GG adducts with higher efficiency than CP-GG adducts (14–16), which might, at least partially, explain the difference in mutagenicity of CP and OX.

We have obtained high-resolution solution NMR structures of the OX-GG adduct (17), the CP-GG adduct and undamaged DNA (18) in the AGGC sequence context and the OX-GG adduct and undamaged DNA duplex (manuscript in preparation) in the TGGT sequence context. These were the first NMR solution structures of the OX-GG adduct and the first structures of any Pt-GG adduct in a DNA sequence context with a purine on the 5′ side of the adduct. While NMR structures were useful in assessing differences in the average conformation of Pt-DNA adducts in solution, molecular dynamic (MD) simulations are needed to assess differences in the conformational dynamics of these Pt-DNA adducts. Consequently, MD simulations were performed on Pt-DNA adducts in the AGGC and TGGA sequence contexts. Data obtained from these studies permit clear distinction between the effects of the Pt-GG intrastrand

adduct, the carrier ligand of the Pt-GG adduct (*cis*-diammine vs. diaminocyclohexane), and the sequence context of the adduct (AGGC vs TGGT (NMR) or TGGA (MD)) on both DNA conformation and conformational dynamics in the vicinity of the adducts.

NMR Solution Structures

Conformational Flexibility on the 5′ Side of the Adduct

Previous studies in our laboratory (17, 18) (manuscript in preparation) and other laboratories (17–20) have shown that imino proton resonance of the 5′G of a Pt-GG adduct is more solvent accessible than that of the 3′G. This data suggests that the DNA may be more distorted and/or flexible on the 5′ side of the adduct.

In addition to the higher solvent exchange rate exhibited by the G6 and G7 imino protons, the T5 imino proton in the TGGT sequence context also possesses a fast exchange rate, which is comparable to that shown by the G6 imino proton (manuscript in preparation). We hypothesize that the distortion and flexibility observed on the 5′-side of the Pt-GG adduct is extended to the 5′-flanking residue base pair, corresponding to the T5·A20 base pair for the OX-GG adduct in the TGGT sequence context. This feature was not observed for undamaged DNA or reported previously for CP-GG adducts in the CGGC sequence context (20) or for either CP- and OX-GG adducts in the AGGC sequence context (17). While those 5′ flanking bases do not possess imino proton signals, their complementary bases (G and T) in the opposing strand do possess imino signals; and no solvent accessibility was observed for those imino protons. This data suggests that the 5′-flanking residue of Pt-GG adducts in the TGGT sequence context may exhibit greater flexibility than that of the CGGC or AGGC sequence contexts. This is best understood in terms of the molecular dynamics studies reported below.

DNA Helical Parameters Common to All Pt-GG Adducts

The CP-GG and OX-GG adducts that we have studied (17, 18) (manuscript in preparation) are similar to all other Pt-GG structures reported to date in that they display an increase in roll at the G6-G7 base-pair step, G6-G7 dihedral angle and overall bend angle compared to undamaged DNA (19–23). We hypothesize that these common conformational features of Pt-GG adducts, which are centered around the G6-G7 base-pair step, are important for recognition of both CP- and OX-GG adducts by DNA-binding proteins. It is logical that the G6-G7 base-pair step would be crucial for the recognition of Pt-GG adducts by DNA-binding proteins. Both mismatch-repair proteins and HMG-domain proteins bend the DNA in the direction of the major groove in part, by inserting an amino acid residue between the base pairs at the center of the bend (which in this case would be the G6-G7 base-pair step) (24–27).

Marzilli et al. (20) reported that all structures of Pt-GG adducts available at that time were characterized by a large positive slide and shift for the base-pair step on the 5′ side of the adduct (which would correspond to the A5-G6 base-pair step for the AGGC sequence and the T5-G6 base-pair step for the TGGT sequence) and concluded that should also be considered as a characteristic of all Pt-GG adducts. Our structures of the CP- and OX-GG adducts in the AGGC sequence context (17, 18) were the first of Pt-GG adducts with a purine on the 5′ side of the adduct, and we did not observe a large positive slide and shift at the A5-G6 base-pair step of those adducts. Furthermore, for the T5-G6 base-pair step of the OX-TGGT adduct we observed a large positive slide, but a slightly negative shift. Thus, while all Pt-GG adducts appear to have significant distortions on the 5′ side of the adduct, the exact nature of these distortions is dependent on both sequence context and the nature of the carrier ligand.

DNA Helical Parameters that Distinguish Between CP and OX-GG Adducts

Comparison of DNA helical parameters of the CP-GG adduct in the AGGC sequence context with the DNA helical parameters of the OX-GG adducts in both the AGGC and TGGT sequenced contexts has also allowed us to identify conformational differences between CP-GG and OX-GG adducts that may be relatively independent of sequence context. Specifically, the CP-GG adduct in the AGGC sequence context differs from both OX-GG adducts in slide, twist, and roll at the G6·C19-G7·C18 base-pair step, shift and slide at the G7·C18-C8·G17 base-pair step, opening for the G7·C18 base pair and G6G7 dihedral angle (Table 1). While structures of Pt-GG adducts in more sequence contexts will need to be examined under the same experimental conditions to confirm that these conformational differences of CP- and OX-GG adducts are independent of sequence contexts, we hypothesize that these differences are important for the sequence-independent, differential recognition of CP- and OX-GG

Table 1 Comparison of DNA helical parameters for CP-DNA and OX-DNA in the AGGC and TGGT sequence contexts

Parameters	CP-AGGC	OX-AGGC	OX-TGGT
G6·C19-G7·C18			
Slide (Å)	−0.55 ± 0.10	−1.36 ± 0.30	−0.95 ± 0.07
Twist (°)	18.4 ± 1.4	25.2 ± 2.0	24.99 ± 2.78
Roll (°)	36.3 ± 3.2	28.3 ± 3.2	46.6 ± 2.3
G7·C18-C/T8·G/A17			
Shift (Å)	−0.99 ± 0.17	−1.24 ± 0.10	−0.44 ± 0.25
Slide (Å)	−0.33 ± 0.13	0.93 ± 0.10	−1.02 ± 0.76
G7·C18			
Opening (°)	−1.24 ± 0.93	5.73 ± 0.53	5.91 ± 1.86
G6-G7			
Dihedral Angle (°)	42.7 ± 3.1	35.6 ± 2.8	38.2 ± 3.1

Table 2 Comparison of DNA helical parameters for OX-DNA in the AGGC and TGGT sequence contexts

Parameters	OX-AGGC	OX-TGGT
A/T5·T/A20-G6·C19		
Shift (Å)	0.17 ± 0.04	–0.31 ± 0.36
Slide (Å)	–0.89 ± 0.10	1.67 ± 0.31
Twist (°)	22.1 ± 1.3	36.7 ± 4.5
G6·C19-G7·C18		
Roll (°)	28.3 ± 3.2	46.6 ± 2.3
G7·C18-C/T8·G/A17		
Shift (Å)	–1.24 ± 0.10	–0.44 ± 0.25
Slide (Å)	0.93 ± 0.10	–1.02 ± 0.08
G6·C19		
Buckle (°)	12.6 ± 2.4	6.8 ± 1.0

adducts by DNA-binding proteins. Most of these conformational differences lie on the 3′ side of the adduct, which is consistent with the observation that the damage-recognition protein HMG1a binds primarily to the 3′ side of the adduct (24).

Finally, comparison of DNA helical parameters between OX-GG adducts in the TGGT and AGGC (17) sequence contexts has allowed us to identify some of the conformational features of the OX-GG adduct that are affected by sequence context. This comparison showed significant differences in the shift, slide, and twist at the A/T5·T/A20-G6·C19 base-pair step, roll at the G6·C19-G7·C18 base-pair step, shift and slide at the G7·C18-C/T8·G/A17 base-pair step, and buckle of the G6·C19 base pair (Table 2). We hypothesize that some of these conformational distortions, which are found on both the 5′ and 3′ side of CP- and OX-GG adducts, influence the affinity of DNA-binding for the Pt-GG adducts and are likely to explain the influence of sequence context on the ability of the DNA-binding proteins to discriminate between CP-GG and OX-GG adducts.

MD Simulations and Differences in Conformational Dynamics

The Effect of the Diaminocyclohexane Ring on N–Pt–N Bond Angles

We then used molecular dynamics simulations to explore differences in the conformational dynamics between OX-GG, CP-GG and undamaged DNA in the AGGC (28) and TGGA sequence contexts. In theoretical terms, the most obvious effects of the diaminocyclohexane ring of oxaliplatin are to constrain the bond angle between the Pt and the two amines of diaminocyclohexane. This can be clearly seen when one compares the conformational range of the four possible N–Pt–N bond angles of CP-GG and OX-GG adducts (Fig. 1). The conformational

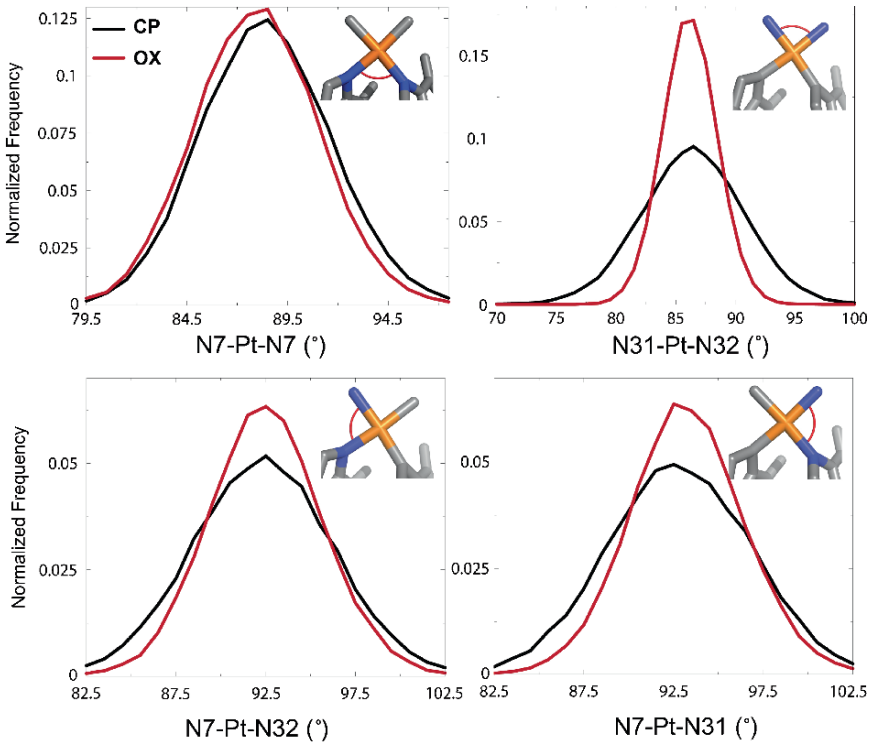

Angles (mean ± SD)

		AGGC	TGGA
CP	N31 -Pt -N32	86.4 ± 4.4	85.7 ± 4.5
	NB1 -Pt -NB2	88.5 ± 3.2	88.7 ± 3.3
	NB1 -Pt -N32	92.7 ± 4.0	93.5 ± 4.2
	NB2 -Pt -N31	92.2 ± 4.0	91.8 ± 4.1
OX	N31 -Pt -N32	86.2 ± 2.3	86.2 ± 2.3
	NB1 -Pt -NB2	88.0 ± 3.1	88.2 ± 3.1
	NB1 -Pt -N 32	93.2 ± 3.2	93.4 ± 3.3
	NB2 -Pt -N31	92.5 ± 3.2	92.0 ± 3.3

Fig. 1 Frequency distribution of platinum bond angles in the AGGC and TGGA sequence contexts. The *upper panel* shows frequency distribution of platinum bond angles in the AGGC sequence contexts. Table compares mean ± standard deviation for the same bond angles in the AGGC and TGGA sequence contexts

dynamics of the NB1(G6N7)–Pt–NB2(G7N7) bond angles are essentially identical for CP- and OX-GG adducts because that bond angle is primarily constrained by the DNA backbone. However, the cyclohexane ring of the OX-GG adduct strongly restricts the conformational range of N31–Pt–N32 bond angle and places modest constraints on the NB1–Pt–N32 and NB2–Pt–N31 bond angles compared to the CP-GG adduct. While the figure only shows bond angles for CP-GG and OX-GG adducts in the AGGC sequence context, these effects were essentially independent of sequence context.

The Effect of N–Pt–N Bond Flexibility and Sequence Context on Hydrogen Bond Occupancy

We next looked at hydrogen bond occupancy (the percentage of time that various hydrogen bonds formed during the simulation). As might be expected, we observed close to 100% occupancy for most of the Watson-Crick hydrogen bonds except for the ones involving the G•C base pairs containing the Pt-GG adduct (G6 and G7). However, we also observed significant formation of hydrogen bonds between the Pt-amines and the surrounding bases. The pattern of hydrogen bond formation was highly dependent on the sequence context of the Pt-GG adduct, and the occupancy of those hydrogen bonds was different for CP-GG and OX-GG adducts. For example, in the AGGC sequence context, the CP-GG adduct preferentially formed hydrogen bonds between the 5′ Pt-amine and A5N7, while the OX-GG adduct preferentially formed hydrogen bonds between the 3′ Pt-amine and G7O6 (Fig. 2). In the TGGA sequence context, the CP-GG adduct preferentially formed hydrogen bonds with A8N7 and the OX-GG adduct with G7O6 and T17O4 (Fig. 3). This data suggests that the greater conformational flexibility of the CP-GG adduct allows it to form hydrogen bonds with the adjacent bases on the same strand of the DNA, while conformation of the OX-GG adduct allows hydrogen bond formation with a 3′ base on the opposite strand of DNA. The obvious question then is how these differences in the pattern of hydrogen bond formation influence DNA conformation.

The Effect of Hydrogen Bond Occupancy on Flexibility on the 5′ side of Pt-GG Adducts

While this difference in conformational flexibility of a 5′ flanking T residue relative to a 5′ flanking A residue in the NMR experiments described earlier is difficult to explain in terms of standard Watson-Crick hydrogen bonds, it is fully consistent with the hydrogen bond occupancy between Pt-amines and the adjacent base pairs

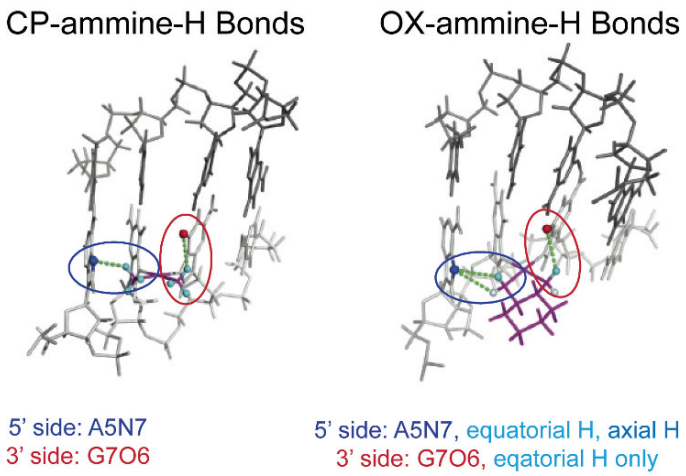

5' side A5N7	3' side G7O6	% H bond occupancy
CP-DNA adduct		
+	–	40.2%
+	+	34.0%
–	+	13.3%
–	–	12.5%
OX-DNA adduct		
+ (ax)	–	7.7%
+ (eq)	–	6.0%
+ (ax)	+	3.5%
+ (eq)	+	40.9%
–	+	34.3%
–	–	7.6%

Total 5′ = 74.2%
Total 3′ = 47.3%
Total 5′ = 58.1%
Total 3′ =78.7%

Fig. 2 Hydrogen bonds between Pt-amine hydrogens and surrounding bases in the AGGC sequence context. Structures illustrating observed hydrogen bond formation are shown in the *upper panel*. Table indicates the percent hydrogen bond occupancy (the % of time that the hydrogen bond is observed during the trajectory) for each of those hydrogen bonds (*see Color Plates*)

observed in molecular dynamic simulations. In the Pt-AGGC simulations, hydrogen bond formation between the Pt-amine hydrogens on the 5′ side of the adduct and the N7 of the 5′A residue was observed between 58% (OX-AGGC adduct) and 74% (CP-AGGC adduct) of the time (28). The formation of this hydrogen bond might be expected to significantly decrease the conformational flexibility of the 5′ A. In contrast, almost no hydrogen bond formation was seen between the 5′ Pt-amine hydrogens and the 5′ T residue for either CP-GG or OX-GG adducts in the TGGA sequence context.

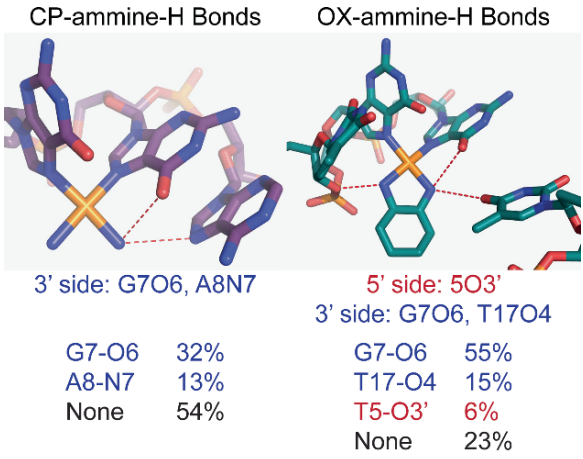

Fig. 3 Hydrogen bonds between Pt-amine hydrogens and surrounding bases in the TGGA sequence context. Structures illustrating observed hydrogen bond formation are shown in the *upper panel*. Table indicates the percent hydrogen bond occupancy (the % of time that the hydrogen bond is observed during the trajectory) for each of those hydrogen bonds (*see Color Plates*)

The Effect of Patterns of Hydrogen Bond Occupancy on DNA Conformation

When we examined the conformational dynamics of DNA helical parameters in the vicinity of the Pt-GG adducts, it was evident that there were some significant differences between CP-GG and OX-GG adducts. For example, in the AGGC sequence context, CP-GG adducts differed from OX-GG adducts in terms of G6·C19 buckle, G6·C19 propeller twist, G7·C18 propeller twist, C8·G17 buckle, A5·T20-G6·C19 slide, G6·C19-G7·C18 slide and G7·C16-C8·G17 slide and shift (28).

To determine whether the conformational dynamics of CP- and OX-DNA adducts might be influenced by the formation of the hydrogen bonds between the Pt-amines and surrounding bases, the trajectory data for DNA helical parameters for the central four base pairs were separated according to patterns of hydrogen bond formation. When this was done, there was clear association between the pattern of hydrogen bond formation for each Pt-GG adduct and the conformational dynamics of the DNA in the vicinity of the adduct. For example, the conformational dynamics of G6·C19 and G7·C18 propeller twist are shown in Fig. 4. When the overall frequency distributions of these parameters are compared (Fig. 4a), one observes subtle differences in the conformational dynamics for CP- and OX-GG adducts. When the frequency distributions of these DNA helical parameters are segregated according to hydrogen bond pattern for the CP-GG adduct (Fig. 4b), the conformation range is clearly different for the A5N7 hydrogen bond on the 5′ side of the adduct compared to the G7O6 hydrogen bond on the 3′ side of the adduct. Similar segregation according to hydrogen bond pattern is observed for the OX-GG adduct (Fig. 4c). Finally, the frequency distributions associated with the most abundant hydrogen bond patterns (A5N7 plus both 5′ and 3′ account for 74.2% of

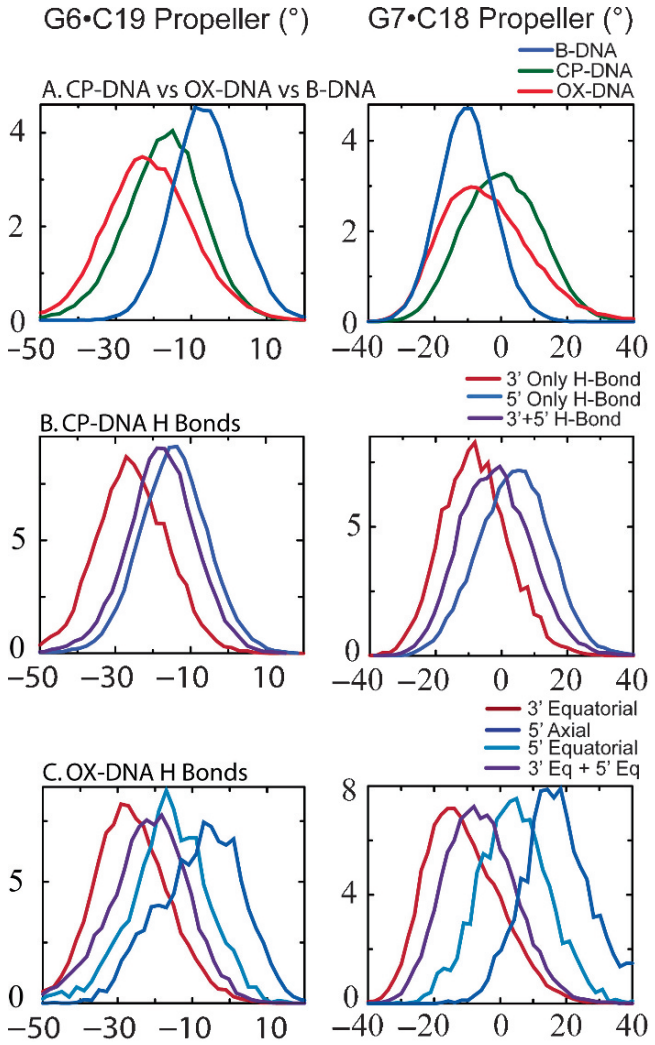

Fig. 4 Effect of patterns of hydrogen bond formation on the frequency distribution of G6·C19 and G7·C18 propeller twist for CP- and OX-GG adducts in the AGGC sequence context. (**a**) Overall frequency distribution for CP-GG (*green*), OX-GG (*red*) and undamaged DNA (*blue*). (**b**) Effect of hydrogen bond pattern on the frequency distribution for CP-GG adducts (5′ A5N7 = *blue*, 3′ G7O6 = *red* & both 5′ and 3′ = *purple*). (**c**) Effect of hydrogen bond pattern on the frequency distribution for OX-GG adducts (5′ axial A5N7 = *blue*, 5′ equatorial A5N7 = *cyan*, 3′ equatorial G7O6 = *red* & both 5′ equatorial and 3′ equatorial = *purple*) (*see Color Plates*)

hydrogen bond occupancy for CP-GG, and G7O6 plus both 5′ and 3′ account for 78.7% of hydrogen bond occupancy for OX-GG) are closely correlated with the overall differences observed in those DNA helical parameters for CP- and OX-GG adducts (Fig. 5).

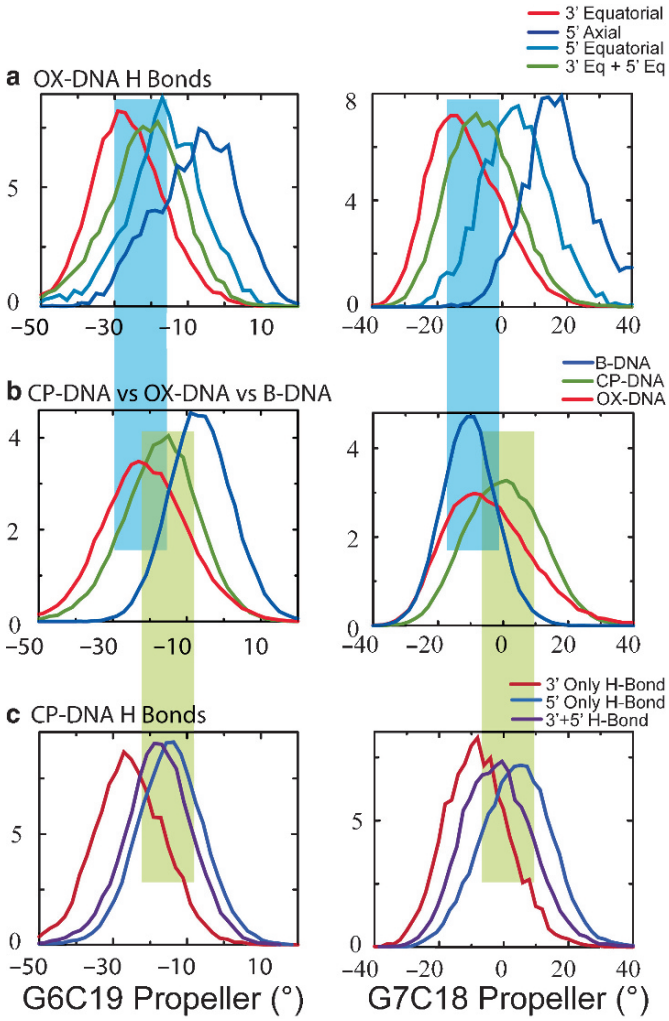

Fig. 5 Correlation between patterns of hydrogen bond formation and differences in the frequency distribution of G6·C19 and G7·C18 propeller twist for CP- and OX-GG adducts in the AGGC sequence context. (**a**) Effect of hydrogen bond pattern on the frequency distribution for OX-GG adducts (5′ axial A5N7 = *blue*, 5′ equatorial A5N7 = *cyan*, 3′ equatorial G7O6 = *red* & both 5′ equatorial and 3′ equatorial = *green*). (**b**) Overall frequency distribution for CP-GG (*green*), OX-GG (*red*) and undamaged DNA (*blue*). (**c**) Effect of hydrogen bond pattern on the frequency distribution for CP-GG adducts (5′ A5N7 = *blue*, 3′ G7O6 = *red* & both 5′ and 3′ = *purple*). *Blue rectangle* indicates correlation between the frequency distribution associated with the most frequently formed hydrogen bonds for OX-GG (total hydrogen bond occupancy for 3′ equatorial plus 3′ and 5′ = 78.7%) and the overall frequency distribution for OX-GG adducts. *Green rectangle* indicates correlation between the frequency distribution associated with the most frequently formed hydrogen bonds for CP-GG (total hydrogen bond occupancy for 5′ A5N7 plus 5′ and 3′ = 74.2%) and the overall frequency distribution for CP-GG adducts (*see Color Plates*)

Conformational Dynamics and the Differential Recognition of CP- and OX-GG Adducts by Damage Recognition Proteins

Data from molecular dynamics simulations suggest a hypothetical model for the differential recognition of CP- and OX-GG adducts by damage recognition proteins and the effect of DNA sequence context on that recognition. We propose that:

1. CP-GG adducts have a greater flexibility with respect to both Pt-amine bond angles and Pt-amine dihedral angles than OX-GG adducts because of constraints imposed by the diaminocyclohexane ring of the OX-GG adduct.
2. This greater flexibility allows the CP-GG adduct to more readily form Pt-amine hydrogen bonds with adjacent bases on the same strand of DNA than OX-GG adducts. At the same time the OX-GG adducts have some unique conformational features that allow them to form Pt-amine hydrogen bonds with bases on the opposite strand than CP-GG adducts.
3. These differences in the patterns of hydrogen bond formation correlate with differences in conformational dynamics that may be important for Pt-DNA adduct recognition by damage recognition proteins.

References

1. Greene MH. Is cisplatin a human carcinogen? J Nat Cancer Inst 1992;84:306–12.
2. Travis LB, Curtis RE, Storm H, et al. Risk of second malignant neoplasms among long-term survivors of testicular cancer. J Natl Cancer Inst 1997;89:1429–39.
3. Silva MJ, Costa P, Dias A, Valente M, Louro H, Boavida MG. Comparative analysis of the mutagenic activity of oxaliplatin and cisplatin in the *Hprt* gene of CHO cells. Environ Mol Mutagen 2005;46:104–15.
4. Bassett E, King NM, Bryant MF, et al. The role of DNA polymerase eta in translesion synthesis past platinum-DNA adducts in human fibroblasts. Cancer Res 2004;64:6469–75.
5. Zdraveski ZZ, Mello JA, Farinelli CK, Essigmann JM, Marinus MG. MutS preferentially recognizes cisplatin- over oxaliplatin-modified DNA. J Biol Chem 2002;277:1255–60.
6. Fink D, Nebel S, Aebi S, et al. The role of mismatch repair in platinum drug resistance. Cancer Res 1996;56:4881–6.
7. Aebi S, Kurdi-Haidar B, Zheng H, et al. Loss of DNA mismatch repair in acquired resistance to cisplatin. Cancer Res 37;3087–90.
8. Fink D, Zheng H, Nebel S, et al. In vitro and in vivo resistance to cisplatin in cells that have lost DNA mismatch repair. Cancer Res 1997;57:1841–5.
9. Vaisman A, Varchenko M, Umar A, et al. The role of hMLH1, hMSH3, and hMSH6 defects in cisplatin and oxaliplatin resistance: correlation with replicative bypass of platinum-DNA adducts. Cancer Res 1998;58:3579–85.
10. Brown R, Hirst GL, Gallagher WM, et al. hMLH1 expression and cellular responses of ovarian tumour cells to treatment with cytotoxic anticancer agents. Oncogene 1997;15:45–52.
11. Wei M, Cohen SM, Silverman AP, Lippard SJ. Effects of spectator ligands on the specific recognition of intrastrand platinum-DNA cross-links by high mobility group box and TATA-binding proteins. J Biol Chem 2001;276:38774–80.

12. Zhai X, Beckmann H, Jantzen H-M, Essigmann JM. Cisplatin-DNA adducts inhibit ribosomal RNA synthesis by hijacking the transcription factor human upstream binding factor. Biochemistry 1998;37:16307–15.
13. Coin F, Frit P, Viollet B, Salles B, Egly JM. TATA binding protein discriminates between different lesions on DNA, resulting in a transcription decrease. Mol Cell Biol 1998;18:3907–14.
14. Vaisman A, Lim SE, Patrick SM, et al. Effect of DNA polymerases and high mobility group protein 1 on the carrier ligand specificity for translesion synthesis past platinum-DNA adducts. Biochemistry 1999;38:11026–39.
15. Vaisman A, Chaney SG. The efficiency and fidelity of translesion synthesis past cisplatin and oxaliplatin GpG adducts by human DNA polymerase beta. J Biol Chem 2000;27:13017–25.
16. Vaisman A, Masutani C, Hanaoka F, Chaney SG. Efficient translesion replication past oxaliplatin and cisplatin GpG adducts by human DNA polymerase eta. Biochemistry 2000;39:4575–80.
17. Wu Y, Pradhan P, Havener J, et al. NMR solution structure of an oxaliplatin 1,2-d(GG) intrastrand cross-link in a DNA dodecamer duplex. J Mol Biol 2004;341:1251–69.
18. Wu Y, Bhattacharyya D, King CL, et al. Solution structures of a DNA dodecamer duplex with and without a cisplatin 1,2-d(GG) intrastrand cross-link: comparison with the same DNA duplex containing an oxaliplatin 1,2-d(GG) intrastrand cross-link. Biochemistry 2007;46:6477–87
19. Yang D, van Bloom SSGE, Reedijk J, van Bloom JH, Wang AHJ. Structure and isomerization of an intrastrand cisplatin-cross-linked octamer DNA duplex by NMR analysis. Biochemistry 1995;34:12912–20.
20. Marzilli LG, Saad JS, Kuklenyik Z, Keating KA, Xu Y. Relationship of solution and protein-bound structures of DNA duplexes with the major intrastrand cross-link lesions formed on cisplatin binding to DNA. J Am Chem Soc 2001;123:2764–70.
21. Herman F, Kozelka J, Stoven V, et al. A d(GpG)-platinated decanucleotide duplex is kinked an extended NMR and molecular mechanics study. Eur J Biochem 1990;194:119–33.
22. Gelasco A, Lippard SJ. NMR solution structure of a DNA dodecamer duplex containing a *cis*-diammineplatinum(II) dGpG intrastrand cross-link, the major adduct of the anticancer drug cisplatin. Biochemistry 1998;37:9230–9.
23. Takahara PM, Frederick CA, Lippard SJ. Crystal structure of the anticancer drug cisplatin bound to duplex DNA. J Am Chem Soc 1996;118:12309–21.
24. Ohndorf UM, Rould MA, He Q, Pabo CO, Lippard SJ. Basis for recognition of cisplatin-modified DNA by high-mobility-group proteins. Nature 1999;399:708–12.
25. Love JJ, Li X, Case DA, Giese K, Grosschedl R, Wright PE. Structural basis for DNA bending by the architectural transcription factor LEF-1. Nature 1995;376:791–5.
26. Werner MH, Huth JR, Gronenborn AM, Clore GM. Molecular basis of human 46X,Y sex reversal revealed from the three-dimensional solution structure of the human SRY-DNA complex. Cell 1995;81:705–14.
27. Murphy EC, Zhurkin VB, Louis JM, Cornilescu G, Clore GM. Structural basis for SRY-dependent 46-X,Y sex reversal: modulation of DNA bending by a naturally occurring point mutation. J Mol Biol 2001;312:481–99.
28. Sharma S, Gong P, Temple B, Bhattacharyya D, Dokholyan NV, Chaney SG. Molecular dynamic simulations of cisplatin- and oxaliplatin-d(GG) intrastrand cross-links reveal differences in their conformational dynamics. J Mol Biol 2007;373:1123–40.